A Structural Basis for Substrate Selectivity and Stereoselectivity in Octopine Dehydrogenase from Pecten maximus

ARTICLE *in* JOURNAL OF MOLECULAR BIOLOGY · SEPTEMBER 2008

Impact Factor: 4.33 · DOI: 10.1016/j.jmb.2008.06.003 · Source: PubMed

4 AUTHORS, INCLUDING:

Sander H J Smits
Heinrich-Heine-Universität Düsseldorf
87 PUBLICATIONS **859** CITATIONS
SEE PROFILE

Lutz Schmitt
Heinrich-Heine-Universität Düsseldorf
130 PUBLICATIONS **3,060** CITATIONS
SEE PROFILE

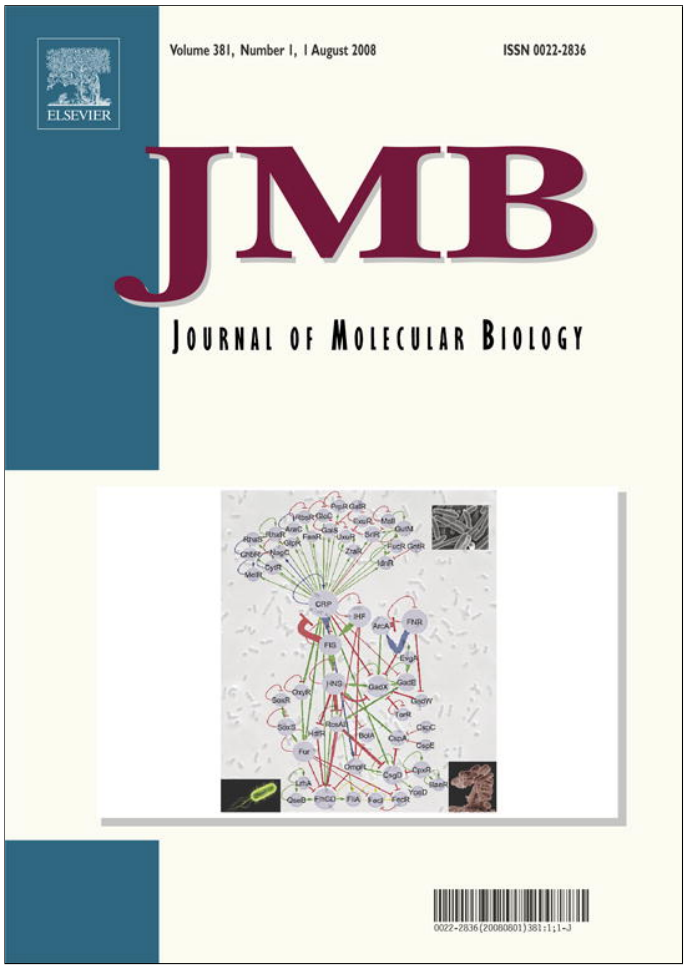

doi:10.1016/j.jmb.2008.06.003 J. Mol. Biol. (2008) 381, 200–211

JMB

Available online at www.sciencedirect.com

ScienceDirect

ELSEVIER

A Structural Basis for Substrate Selectivity and Stereoselectivity in Octopine Dehydrogenase from *Pecten maximus*

Sander H. J. Smits[1]†, Andre Mueller[2]†, Lutz Schmitt[1]* and Manfred K. Grieshaber[2]

[1]*Institute of Biochemistry, Heinrich Heine University, Universitaetsstrasse 1, 40225 Duesseldorf, Germany*

[2]*Institute of Zoophysiology, Heinrich Heine University, Universitaetsstrasse 1, 40225 Duesseldorf, Germany*

Received 13 April 2008; received in revised form 26 May 2008; accepted 1 June 2008
Available online 7 June 2008

Edited by G. Schulz

Octopine dehydrogenase [N^2-(D-1-carboxyethyl)-L-arginine:NAD^+ oxidoreductase] (OcDH) from the adductor muscle of the great scallop *Pecten maximus* catalyzes the reductive condensation of L-arginine and pyruvate to octopine during escape swimming. This enzyme, which is a prototype of opine dehydrogenases (OpDHs), oxidizes glycolytically born NADH to NAD^+, thus sustaining anaerobic ATP provision during short periods of strenuous muscular activity. In contrast to some other OpDHs, OcDH uses only L-arginine as the amino acid substrate. Here, we report the crystal structures of OcDH in complex with NADH and the binary complexes NADH/L-arginine and NADH/pyruvate, providing detailed information about the principles of substrate recognition, ligand binding and the reaction mechanism. OcDH binds its substrates through a combination of electrostatic forces and size selection, which guarantees that OcDH catalysis proceeds with substrate selectivity and stereoselectivity, giving rise to a second chiral center and exploiting a "molecular ruler" mechanism.

Keywords: protein-ligand complex; stereoselectivity; proton relay system; X-ray crystal structure; scallop

Introduction

A spectacular feature of the great scallop *Pecten maximus* is its prowess as a swimmer when escaping a predating star fish. Work during jet propulsion swimming is performed by contractions of a single adductor muscle located in the middle of the valves.[1] It gains its energy from the transphosphorylation of phospho-L-arginine and anaerobic glycolysis, which is terminated by octopine [N^2-(D-1-carboxyethyl)-L-arginine], a prototype of opines.[2] In the adductor muscle, octopine dehydrogenase [N^2-(D-1-carboxyethyl)-L-arginine:NAD^+ oxidoreductase] (OcDH; EC 1.5.1.11) catalyzes the formation of octopine via the reductive condensation of L-arginine and pyruvate in the presence of NADH.[3]

Various opines have been isolated from phylogenetic diverse sources, such as bacteria, yeast, plant tumors and marine invertebrates.[4] For example, in the amino acid pool of *Streptococcus lactis* subsp. *lactis*, N^5-(1-L-carboxyethyl)-L-ornithine and the higher homologue N^5-(1-L-carboxyethyl)-L-lysine were detected.[5,6] Saccharopine [N^6-(L-1,3-dicarboxypropyl)-L-lysine] is a key compound in the α-amino adipate pathway for L-lysine biosynthesis in *Saccharomyces cerevisiae*.[7] In crown gall tumors of plants, different opines resulting from the expression of tumor-inducing plasmids of *Agrobacterium tumefaciens* in plants are found. The opines serve as nutrients for the infecting bacteria.[8,9] Many invertebrate species accumulate opines in the muscle tissues during fight-and-flight reactions.[2]

The different opines are produced during a reductive condensation of the α- or ω-amino moiety of an L-amino acid with an α-keto acid,[4] catalyzed by various opine dehydrogenases (OpDHs) using NAD(P)H as a co-substrate. In many invertebrates, in

*Corresponding author. E-mail address: lutz.schmitt@uni-duesseldorf.de.

† S.H.J.S. and A.M. contributed equally to this work.

Abbreviations used: CENDH, *N*-(1-D-carboxyethyl)-L-norvaline: NAD^+ oxidoreductase; LDH, lactate dehydrogenase; MDH, malate dehydrogenase; OcDH, octopine dehydrogenase [N^2-(D-1-carboxyethyl)-L-arginine: NAD^+ oxidoreductase]; OpDH, opine dehydrogenase; SAD, single anomalous dispersion.

particular, in some marine species of Annelida and Mollusca, OpDHs terminate anaerobic glycolysis, as does lactate dehydrogenase (LDH) in Crustacea, Insecta and Vertebrata.[2] In all animal examples known so far, this reaction oxidizes glycolytically born NADH to NAD^+, thereby sustaining anaerobic ATP provision during short periods of strenuous muscular activity. Five OpDHs have been characterized based on their activities,[2,10] and they can be distinguished by their amino acid substrate: OcDH; alanopine dehydrogenase [N^2-(D-1-carboxyethyl)-L-alanine:NAD^+ oxidoreductase] (EC 1.5.1.17); strombine dehydrogenase [N^2-(D-1-carboxyethyl)-glycine:NAD^+ oxidoreductase] (EC 11.5.1.22); tauropine dehydrogenase (taurine; EC 1.5.1.23); and β-alanopine dehydrogenase [N^2-(D-1-carboxyethyl)-L-alanine:NAD^+ oxidoreductase] (EC 1.5.1.26).

Furthermore, OpDHs are potential candidates for enzyme-based chiral synthesis due to their capability of forming one new chiral center with perfect selectivity from one chiral precursor and one achrial precursor.[11] Applications of opines as enzyme potentiators or inhibitors have been described for bradykinin or the angiotensin-converting enzyme.[4]

In order to elucidate the three-dimensional structure of animal OpDHs and, consequently, the reaction mechanism of OpDHs, we chose the easily accessible OcDH from the adductor muscle of the great scallop *P. maximus*, since much is known about the distribution and physiological function of this enzyme.[2] In 1969, OcDH was the first OpDH to be purified to near homogeneity.[12] In solution, most OpDHs have a monomeric structure between 37 and 45 kDa. The maximal reaction rate in the direction of opine formation is found at pH 6.5–7.5, and that in the reverse direction is found at pH 8.0–9.5[13]; a putative reaction mechanism derived from kinetic studies supposedly constitutes an ordered ter–bi system with NADH binding first, followed by random binding of pyruvate and the respective L-amino acid.[14] The reductive condensation reaction of L-arginine with pyruvate is interesting, because a second chiral center is formed and, as a corollary, OpDHs display either (D,L) or (L,L) specificity. Amino acid analysis has established that enzymes catalyzing product formation with (D,L) stereochemistry and those catalyzing product formation with (L,L) stereochemistry belong to two distinct protein subfamilies.[15] Furthermore, among one subfamily, sequence homology is around 20%–30%, while no significant homology exists between the two subfamilies.

Recently, cloning and heterologous overexpression of OcDH from *P. maximus* were accomplished, allowing site-directed mutagenesis.[16] This initial analysis suggested the presence of a catalytic triad composed of His212, Asp329 and Arg324. Although these studies of OcDH were important to determine critical key amino acids of the active site and to postulate a putative reaction mechanism, a three-dimensional structure of OcDH is required to fully comprehend this enzyme and utilize its capabilities.

Here, we report the crystal structures of the OcDH–NADH complex and the two binary complexes OcDH–NADH/L-arginine and OcDH–NADH/pyruvate. Based on these data, the molecular principles leading to octopine formation can be rationalized and thus the question concerning substrate selectivity and stereoselectivity in OcDH can be answered.

Results and Discussion

Structure determination

The structure of the binary OcDH–NADH complex was determined initially to a resolution of 2.8 Å by a single anomalous dispersion (SAD) experiment using selenomethionine-incorporated protein. An electron density map was obtained from the SAD data set (Table 1), which was of sufficient quality to build a model, subsequently refined with REFMAC5.[18] This data set allowed us to correctly build all amino acids except the starting methionine. The model then served as a template to phase the high-resolution data set at 2.1 Å through molecular replacement. The high-resolution structure was further refined (REFMAC5[18]) together with several rounds of manual rebuilding using Coot.[21] The quality of the electron density allowed automatic water picking by Arp/Warp,[22] which was manually checked for correctness. The structures of the binary complexes OcDH–NADH/L-arginine and OcDH–NADH/pyruvate were determined by molecular replacement employing the 2.1-Å structure of the OcDH–NADH complex as a template. In the OcDH–NADH/pyruvate structure, however, the density of one loop (amino acids 281–290; see below) was of poor quality and therefore excluded from the final model. A summary of the collected data, refinement statistics and model contents is given in Table 1.

Overall structure

OcDH is composed of two domains of equal size separated by a deep cleft (Fig. 1). Domain I consists of residues 1–199 (shown in green in Fig. 1), which form a central eight-stranded β-sheet of a mixed parallel and anti-parallel character flanked by α-helices as well as by a small four-stranded β-sheet containing both parallel and anti-parallel strands. Part of the eight-stranded β-sheet is organized as a six-stranded parallel sheet. It contains a classic α-unit resembling the NAD binding helix separating the first two β-strands. The amino acid sequence of the loop joining the first β-strand to helix α1 includes the glycine-rich region GGGNGA. This sequence fits to the consensus sequence GXGXXG/A, which delineates the co-substrate binding site in dehydrogenases.[23] Domain I is connected to the N-terminus of domain II via a so-called type 1 connection,[24] and both domains together build up the L-arginine and pyruvate binding site. Domain II (shown in blue in Fig. 1), which consists of 204 amino acids (residues 200–399 and the His_5 tag), starts with a short helix–kink–helix (helix α8 and helix α9), followed by two

Table 1. Crystallographic parameters

	Selenomethionine	Native (NADH)	Pyruvate (NADH)	L-Arginine (NADH)
Crystal parameters at 100 K				
Space group	$P4_12_12$	$P4_12_12$	$P4_12_12$	$P4_12_12$
Unit cell parameters (Å)				
a, *b*, *c*	99.1, 99.1, 125.7	99.8, 99.8, 126.5	95.9, 95.9, 117.9	95.0, 95.0, 120.2
Data collection and processing				
Wavelength (Å)	0.97854	0.97854	0.8148	0.8348
Resolution (Å)	20–2.75 (2.75–2.8)	20–2.1 (2.1–2.15)	20.0–2.6 (2.60–2.7)	20.0–3.1 (3.2–3.1)
Mean redundancy	8.4 (3.8)	5.1 (2.5)	6.1 (6.3)	6.9 (7.0)
Unique reflections	24,818	37,905	17,525	71,952
Completeness (%)	93.0 (96.5)	93.0 (96.5)	99.9 (99.8)	99.5 (99.9)
I/σ	6.8 (3.0)	6.8 (3.0)	26.91 (5.1)	13.0 (5.9)
R_{merge} [a]	16.4 (28.8)	15.8 (38.0)	6.2 (36.0)	16.2 (36.4)
Wilson *B*-factor (Å^2)	28.2	22.8	47.5	44.3
Refinement				
R_F [b] (%)		20.5	25.2	19.5
R_{free} [c] (%)		25.0	29.0	24.0
rmsd from ideal				
Bond lengths (Å)		0.09	0.004	0.06
Bond angles (°)		1.079	0.808	0.978
Average *B*-factors (Å^2)				
Protein		21.5	36.9	23.6
Substrate			50.6	39.5
Ramachandran plot				
Most favored (%)		100	94.2	96.4
Allowed (%)			5.4	3.6
Generously allowed (%)			0.4	
Disallowed (%)				
Monomers/ASU		1	1	1
Protein residues		2–404	2–280, 291–404	2–404
Ligand		1 NADH	1 NADH, 1 pyruvate	1 NADH, 1 arginine
Others		8 ethylene glycol, 251 water		

Crystal parameters and data collection statistics were derived from XDS.[17] Refinement statistics were obtained from REFMAC5,[18] and Ramachandran analysis was performed using PROCHECK.[19,20]

[a] R_{sym} is defined as $R_{sym} = \sum_{hkl}\sum_{i}\left|I_i(hkl)-\langle I(hkl)\rangle\right| / \sum_{hkl}\sum_{i} I_i(hkl)$.

[b] R_F is defined as $R_f = \sum_{hkl}||F_{obs}|-|F_{calc}|| / \sum_{hkl}|F_{obs}|$.

[c] R_{free} is calculated as R_F but for 5% randomly chosen reflections that were omitted from all refinement steps.

anti-parallel β-strands. The structure continues with a bundle of α-helices, one of which is very long (amino acids 232–264), giving the second domain its rigid structure. The C-terminal His_5 tag of a symmetry-related molecule protrudes into the cleft between the two domains and introduces a stabilizing crystal contact. However, it does not interfere with substrate binding, which was achieved by soaking NADH-bound OcDH crystals with L-arginine or pyruvate (see below).

The NADH binding site

The binding site of the co-substrate NADH was identified by analyzing the initial electron density from the 2.8-Å SAD data set. NADH is bound to the Rossmann fold by interactions typically observed in dehydrogenases (Table 2).[25] While the pyrophosphate moiety interacts with Asn12 and Gly13 of the consensus sequence GGGNGA, Phe35, Glu38 and Gly10 establish further interactions with the co-substrate. Here, Phe35 undergoes phi–phi stacking with the adenine ring and Glu38 forms a hydrogen bond with the hydroxyl groups of the ribose ring. Gly10, which is part of the consensus motif of dinucleotide binding proteins, also interacts with the ribose moiety of NADH. However, during initial rounds of refinement, it became apparent that the nicotine amide moiety adopts the syn conformation. Such a rather unusual conformation of the NADH co-factor was already proposed for OcDH in the early 1970s,[26–28] but our analysis provides the first structural evidence that OcDH indeed binds NADH in the syn conformation. As shown in Fig. 2, this syn conformation of NADH is only stabilized by interactions of the amide group with the backbone oxygen and nitrogen of Cys148 (highlighted as sticks in Fig. 2). Obviously, the syn conformation suggests that the hydride transfer from NADH to the Schiff base adduct between L-arginine and pyruvate occurs from the pro-*S* site, similar to OcDHs found in crown gall tumors.[29]

The binary OcDH–NADH/L-arginine complex

In contrast to the OcDH–NADH complex, which was co-crystallized, the binary complex OcDH–

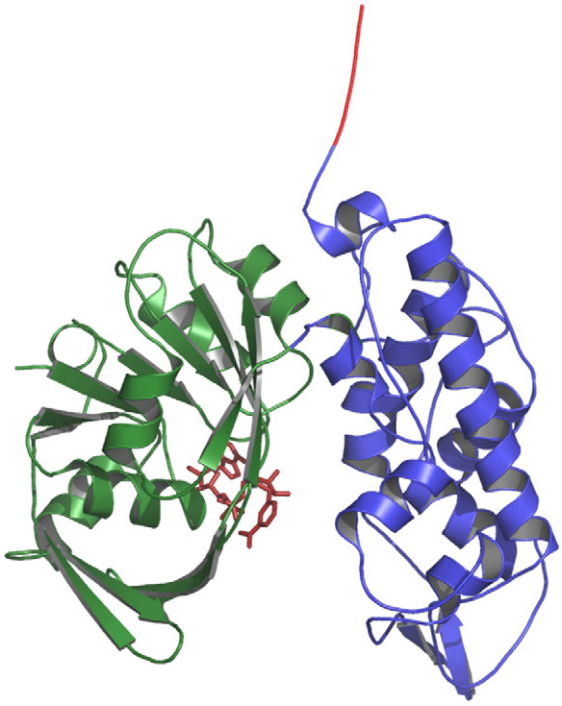

Fig. 1. Overall structure of OcDH. Domain I, consisting of the Rossmann fold, is depicted in green (amino acids 2–199). Domain II, the "arginine binding" domain, is depicted in blue (amino acids 200–404). The co-factor NADH is highlighted in red and shown in stick representation. Shown in red are the five histidine residues of the tag. For simplicity, water molecules are not shown.

NADH/L-arginine was obtained through soaking of L-arginine into preformed OcDH–NADH crystals (see Materials and Methods for details and Table 1). This obviously raised the question of whether this complex reflects a physiological situation. In the OcDH–NADH/L-arginine binary complex (Fig. 2), NADH is bound to OcDH in a fashion identical with that for the OcDH–NADH complex and stabilized in the syn conformation through equal interactions with the backbone of Cys148. The substrate L-arginine, which is located above His212, is coordinated via a hydrogen bond between its α-carboxyl oxygen and the N3 of His212 as well as via hydrogen bonds of the α-amino group with the backbone of Tyr208, contributing directly to substrate binding (Fig. 2; further details are given in Table 2). The guanidinium group, on the other hand, is fixed inside the binding pocket via a salt bridge with Glu142 (highlighted in green in Fig. 2), van der Waals interactions with Trp278 and hydrogen bonds with the backbone carbonyl of Met206. While His212, Trp278 and Met206 are located in domain II, Glu142 is part of domain I, suggesting that L-arginine binding involves both domains of OcDH and likely triggers a domain closure. Such a motion is further supported by the fact that Met206, Tyr208 and His212 are located in a rather flexible helix–kink–helix motif that forms the N-terminal part of domain II (for further details, see below). N3 of His212, which participates in ligand binding, is coordinated by Asp329 via a hydrogen bond forming the Asp–His proton relay system.[30] These interactions are supported by mutagenesis studies and demonstrate that the binary complex obtained by soaking reflects the natural state.[16] More important, however, is that Arg324, which has been proposed to be part of a catalytic triad similar to LDH or malate dehydrogenase (MDH),[30,31] is too remote to participate in L-arginine binding.

In all OpDHs identified so far in invertebrates, residues His212 and Asp329 are conserved, supporting the idea of a general catalytic mechanism (Table 3). Although Glu142 and Trp278 are conserved as well, the L-amino acid substrate differs in the various members of the OpDH family, which may require a particular mechanism for substrate recognition and selection. The only other available three-dimensional structure of an enzyme of the OpDH superfamily is that of the apo form of *N*-(1-D-carboxyethyl)-L-norvaline:NAD^+ oxidoreductase (CENDH) from *Arthrobacter* sp. strain 1C.[32] CENDH catalyzes the NADH-dependent reductive condensation of hydrophobic L-amino acids, such as L-methionine, L-isoleucine, L-valine, L-phenylalanine and L-leucine, with α-keto acids, such as pyruvate, glyoxylate, α-ketobutyrate and oxaloacetate with (D,L) specificity.[33] Crystals of CENDH were obtained in the presence of NAD^+. Although no co-factor could be assigned in the final electron density, this structure allowed an analysis of the reaction mechanism and the principles of governing substrate selection.

CENDH forms a homodimer, already suggesting profound structural differences with regard to substrate selection in OcDH. CENDH possesses a similar binding site as OcDH that is composed of His202, Asp297 and Trp258. In the former enzyme, however, the side chain of Val197 points into the putative substrate binding site. Therefore, only substrates such as norvaline or small hydrophobic amino acids are

Table 2. Summary of the interactions of NADH with OcDH

	Residue	Interaction	Distance (Å)
NADH binding	NADH		
	C2	Phe35 (CD1)	3.5
	AO2*	Glu38 (OE1)	3.1
	AO3*	Glu38 (OE2)	3.1
		Gly10 (O)	3.1
Pyrophosphate 1 (AP)	AO2	Asn12 (N)	3.2
		Asn12 (ND2)	3.4
Pyrophosphate 2 (NP)	NO1	Asn12 (ND2)	3.2
	NO2	Gly13 (N)	2.9
Nicotine amide ring	NO7	Cys148 (N)	3.2
	NN7	Cys148 (O)	3.6
L-Arginine (substrate)	OXT	His212 (N3)	2.9
	N1	Tyr208 (O)	3.4
		Ser207 (O)	3.6
	Cb	Ser207 (O)	3.2
	CD1	Trp278 (CH2)	3.6
	NH2-1	Trp278 (CE2)	3.2
		Trp278 (CE2)	3.5
		Met206 (O)	2.7
	NH1	Met206 (O)	3.4
		Glu142 (OE1)	3.1
Pyruvate	O3	His212 (N3)	3.0
	O2	Gln118 (NE2)	3.6

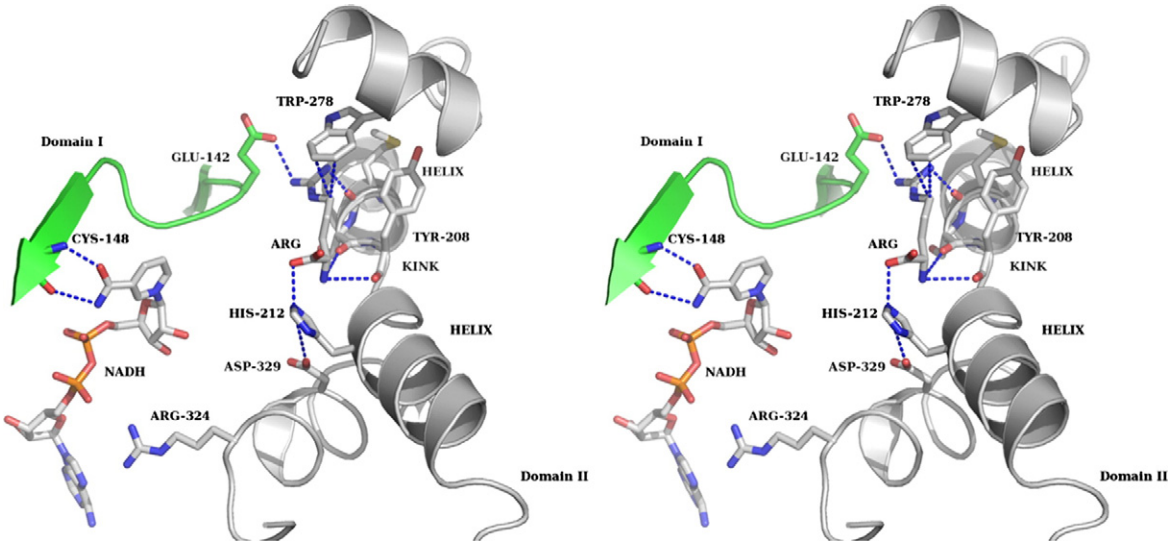

Fig. 2. Stereoview of the arginine binding pocket. The arginine binding pocket is located in domain II, directly at the N-terminal helix–kink–helix motif of domain II. The side chain of arginine is coordinated by Trp278, backbone interactions with Tyr208 (domain II) and those with Glu142 (domain I). The C^{α} of L-arginine is bound by His212 of the Asp–His dyad. NADH is bound in a canonical fashion (Table 2) to the Rossmann fold, while interactions of the amide side chain of the nicotine amide ring with the backbone atoms of Cys148 (domain I) ensure the syn conformation.

accommodated in the assumed binding site of CENDH.[34] In clear contrast, the corresponding amino acid in OcDH (Tyr208 located in the kink of the helix–kink–helix motif) is flipped out of the binding site, allowing the large side chain of L-arginine to bind efficiently. Val197 is part of a helix, while Tyr208 is located in a kink. However, both catalytically important histidine residues (His212 in OcDH and His202 in CENDH) superimpose perfectly, which is achieved by the presence of a single amino acid gap in the sequence of OcDH as shown by the corresponding alignment (Table 3). Thus, the positioning of the respective side chains of Val197 and Tyr208 in CENDH and OcDH generates a "molecular ruler" that distinguishes substrates based on size, a simple but effective mechanism.

The binary OcDH–NADH/pyruvate complex

In the binary OcDH–NADH/pyruvate complex (Fig. 3), which was obtained via soaking of pyruvate into preformed OcDH–NADH crystals, pyruvate is coordinated through Gln118 (domain I) and His212 (domain II). The side chain of Gln118 coordinates the carboxyl moiety of pyruvate, whereas His212 imposes orientation restraints and interacts with the carbonyl group via a hydrogen bond. The importance of Gln118 is emphasized by mutational analysis. Mutation of Gln118 to alanine or aspartate resulted in drastically reduced enzymatic activities, affecting both k_{cat} and K_m (Table 4). Comparison of alanine and aspartate mutants revealed that the introduction of a negative charge (Q118D) had a more pronounced effect on the catalytic efficiency (k_{cat}/K_m) for pyruvate (factor of 10^4) than for L-arginine (factor of 10^3) and NADH (factor of 10^2). In the light of the structure of the binary complex, these mutational data can be rationalized, because the introduction of a negative charge in the binding pocket (Q118D) resulted in a pronounced reduction of activity due to repulsive interactions between aspartate and pyruvate.

The binding site is optimally suited for pyruvate as a substrate since prolongation by but a single methylene group reduced activity (Table 5), as demonstrated for α-ketobutyrate reducing the catalytic efficiency of OcDH by a factor of 10 and for α-ketovalerate (containing two extra methylene groups) reducing it by a factor of 200. Obviously, α-keto acid extended by one or two methylene units are already too long to fit into the binding site, which is built up by voluminous Gln118 and His212. As a corollary, Gln118 is conserved in all invertebrate OpDHs that employ pyruvate as an α-keto acid (Table 3).

The presence of residues Gln118 and His212, which are conspicuously placed in domain I and domain II, respectively, facilitates pyruvate binding with a concomitant domain closure stabilizing substrate arrangement for the reductive condensation of L-arginine and pyruvate. This joint reaction mode between the two domains can also explain the reduced enzymatic activity in the presence of α-ketobutyrate and α-ketovalerate, since their size prevents complete domain closure required for an efficient hydride transfer and, consequently, for high enzymatic turnover numbers. Due to the three-dimensional orientation of the active center, OcDH can accommodate high anaerobic flux rates of ATP provision necessary during escape swimming in *P. maximus*.

In contrast to all invertebrate OpDHs known so far, the bacterial CENDH possesses an alanine (Ala111) at the position of Gln118 (Table 3), which makes CENDH rather promiscuous with respect to the α-keto acids. It employs pyruvate, glyoxylate, α-ketobutyrate or oxaloacetate with similar efficiencies.[34] Since pyruvate is bound to OcDH via interactions with His212 and Gln118, the difference at position 118 suggests

Table 3. Sections of a protein sequence alignment for different OpDHs

	Δ		Δ		Δ ◇		Δ		◇ ◇	
Pecten maximus ODH	IVGLPSQAGFE	122	MSFETLPWACR	149	IMSYS-FVHPA	214	DIYQWYLEY	282	DFGNRYLTEDIPMGM	334
Mizuhopecten yessoensis ODH	IVGLPSQAGFE	122	MSFETLPWACR	149	IMSYS-FVHPA	214	DIYQWYLEY	282	DFGNRYLTEDIPMGM	334
Loligo vulgaris ODH	IVGLPSQPGFQ	131	VSFESLPWACR	158	LLADA-VVHPP	224	HLFDWYKLN	292	DFTYRYMTEDIPFGM	345
Loligo opalescens ODH	IVGLPSQPGFQ	130	VSFESLPWACR	157	LLADA-VVHPP	223	HLFDWYKLN	291	DFTYRYMTEDIPFGM	344
Sepia officinalis ODH	IVGLPSQPGFQ	131	VSFESLPWACR	158	LLADS-VVHPP	224	HLFDWYKLN	292	DFNYRYMTEDIPFGM	345
Pseudocardium sachalinensis ODH	IVGLPGQPGFE	128	MSIETLPWACR	155	FLYRP-TVHPP	223	SMQDCFIGE	291	DFKYRYLMEDVPYGL	344
Haliotis discus hannai TDH	IVGMPGQPGFE	127	MSFESLPWACR	154	LATKS-IIHPP	220	HLYDWYLRD	288	DFRYRYLTEDVPNGL	341
Arabella iricolor TDH	VVGFPGQPGFD	121	MNFVSLPWACR	148	IMAVNGMLHPS	215	HMHPYYIGA	283	DFTGRYFGEDIPFGL	336
Fusitriton oregonensis AloDH	IIGLPGQPGFE	124	LSYESLPWACR	151	LMTKS-IVHPP	217	HLLEWYRQD	285	DFGYRYLAEDIPFGL	338
Marphysa sanguinea AloDH	LVGLPGQPGFE	123	MAFESLPWACR	148	LMSVNSYIHSS	215	HVLQWYLRV	283	NFKHRYLSEDIPYGL	336
Marphysa sanguinea StrDH	LVGLPGQSGFE	123	MSFESLPWACR	148	LMATNGYIHPS	215	HIWQWYLRV	283	DFKHRYLMEDIPFGL	336
Arthrobacter spec. CENDH	IILNPGATGGA	115	GETSSMLFTCR	143	LTNVNAVMHPL	204	SVCEWYKES	262	NLNTRYFFEDVSTGL	302

Protein sequences used are OcDHs from *P. maximus*, *Mizuhopecten yessoensis*, *Loligo vulgaris*, *Loligo opalescens*, *Sepia officinalis* and *Pseudocardium sachalinensis*; tauropine dehydrogenases from *Arabella irricolor* and *Haliotis discus hannai*; the annotated alanopine dehydrogenase from *Fusitriton oregonensis*; the alanopine dehydrogenase and strombine dehydrogenase from *Marphysa sanguinea*; and the CENDH from *Arthrobacter* sp. strain 1C. Highlighted in red are the amino acids involved in the binding of L-arginine (in OcDH: Glu142 and Trp278) and pyruvate (Gln118), and highlighted in green are the His–Asp dyad (in OcDH: His212 and Asp329) and a functionally important L-arginine (in OcDH: Arg324). For sequence alignment, ClustalW was used [http://www.ebi.ac.uk/CLUSTALW].

that CENDH employs a binding mode different from OcDH or that the carboxylate moiety in CENDH is not specifically recognized.

Comparison of OcDH with related crystal structures of dehydrogenases

Currently, the structure of CENDH from *Arthrobacter* sp. strain 1C[32] is the only other known crystal structure of the OpDH superfamily that catalyzes the reductive condensation of an L-amino acid with an α-keto acid. CENDH shows a broader substrate specificity with a putative active site located only in domain II (see below). Structural superposition of OcDH and CENDH (data not shown) did not highlight any gross differences in the overall structure. The NADH/NAD binding site reveals similar interactions of the pyrophosphate moieties with the asparagine and glycine residues located in the Rossmann motif. Whereas the orientation of the nicotinamide hydroxyl group in OcDH is coordinated by the backbone of Cys148 (see above), the density of the nicotinamide ribose group in CENDH was of moderate quality and could not be assigned.

No other dehydrogenase containing the Rossmann fold revealed any structural similarity to OcDH as detected by the Dali server.[35] Even saccharopine dehydrogenase from *S. cerevisiae*,[36,37] which catalyzes the oxidative cleavage of saccharopine to α-ketoglutarate and L-lysine, does not possess a related structure. MDH and LDH, which are members of the α-keto acid dehydrogenase family, contain an Asp–X–X–Arg motif at their active sites that binds the carboxylate group of the α-keto acid. It guarantees the correct orientation of the substrate within the active site.[30] Together with a histidine residue, these amino acids form a His–Asp–Arg triad, which is important for the transfer of the hydride ion from NAD(P)H to the carbonyl group of the α-keto acid.[30,31] Mutational analysis and sequence motif analysis of OcDH revealed the presence of a similar motif (His212–Asp329–Arg324) in domain II,[16] suggesting possible mechanistic similarities between OcDH and LDH/MDH. However, as revealed by these current studies, the arginine residue of OcDH (Arg324) does not participate in either L-arginine (Fig. 2) or pyruvate (Fig. 3) binding. A triad in OcDH does not exist, which implies that this dehydrogenase employs a reaction mechanism different from that in MDH or LDH.

A catalytic dyad combined with an "L-arginine sensor"

The importance of Arg324 in OcDH has recently been demonstrated by mutational analysis, and a canonical His–Asp–Arg triad was proposed.[16] However, the crystal structure suggests that Arg324 is not involved in substrate binding (neither L-arginine nor pyruvate). Rather, it plays a crucial role due to its close proximity to the pyrophosphate moiety of NADH in domain closure.[28] A comparison of the OcDH–NADH (shown in green in Fig. 4a) and the OcDH–NADH/L-arginine (shown in blue in Fig. 4a)

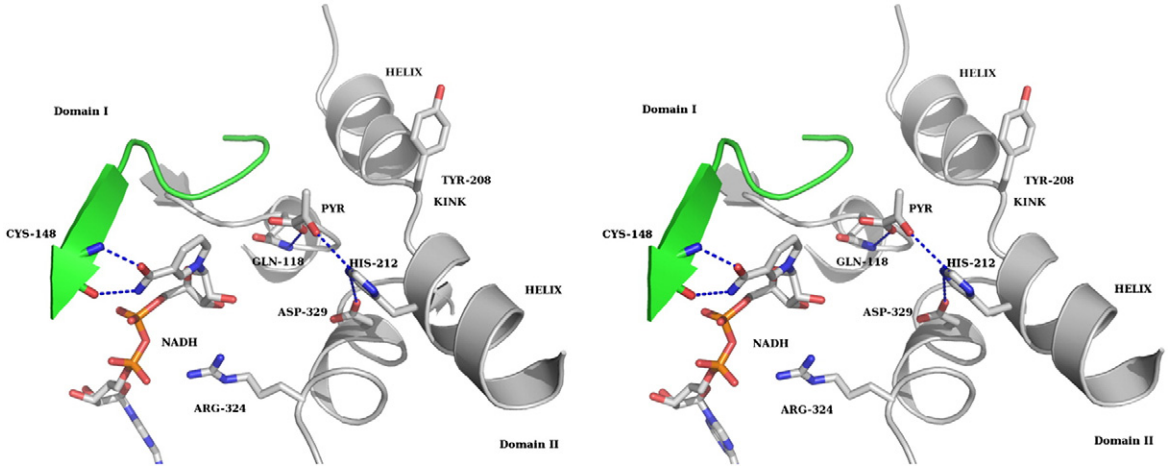

Fig. 3. Stereoview of the pyruvate binding site. Pyruvate is bound by His212 in domain II and by Gln118 in domain I with distances of 3.1 and 2.8 Å, respectively. For further details, see the text.

complexes revealed a 42° rotation of domain II toward the NADH binding domain (domain I) in the latter complex as calculated using the DynDom server.[38] This domain closure is triggered by the interaction of Arg324 (domain II) with the pyrophosphate moiety of NADH bound to the Rossmann fold in domain I. In the OcDH–NADH complex, the distance between Arg324 and the pyrophosphate moiety of NADH is 4.3 Å (Fig. 4b). In the binary complexes of OcDH–NADH/L-arginine and OcDH–NADH/pyruvate, this distance shortens to 3.6 and 3.2 Å, respectively, increasing the strength of the salt bridge interaction (Fig. 4b) and points to a "sensor role" for Arg324. In horse liver alcohol dehydrogenase, a similar Arg–NADH interaction is observed. Here, the strength of the salt bridge is thought to be responsible for domain closure as well as subsequent relaxation after catalysis.[39] This argues against the general diffusion model proposed for domain closure in proteins.[40] It rather suggests that OcDH possesses a catalytic dyad and that the Arg324 sensor stabilizes a productive conformation of OcDH.

Stable binding of NADH to the Rossmann fold of domain I, the first step in the reaction sequence of OcDH, occurs without participation of domain II. A comparison of the two binary complexes implies that both pyruvate and L-arginine are capable of triggering domain closure to a similar extent. However, in the OcDH–NADH/pyruvate complex, pyruvate partially blocks the entrance for L-arginine, while in the OcDH–NADH/L-arginine complex, the accessibility of the pyruvate binding site is not restricted by L-arginine. Thus, it is likely that L-arginine binds to the OcDH–NADH complex in a consecutive step and induces a rotational movement of domain II toward domain I. This semi-closed active center, which is further stabilized using the pyrophosphate moiety of the bound co-substrate and by interactions of L-arginine with residues from both domains (Figs. 2 and 3), is then poised to accept pyruvate; consequently, the

Table 4. Kinetic parameters of the forward reaction (NADH oxidation) catalyzed by recombinant wild-type OcDH and Gln118 mutants

	V_{max} (μmol min^{-1} mg^{-1})	K_m (mmol L^{-1})	$K_{m,\ mut}/K_{m,\ wt}$	k_{cat} (s^{-1})	k_{cat}/K_m (L^*mol^{-1} S^{-1})
Pyruvate					
Wild type[#]	1074	0.77	1	775	1.0×10^{6}
Q118A	393	27	35	283	1×10^{4}
Q118D	101	162	208	73	4.5×10^{2}
L-Arginine					
Wild type[#]	886	0.5	1	640	1.28×10^{6}
Q118A	166	5.8	11	120	2.1×10^{4}
Q118D	169	81	153	122	1.5×10^{3}
NADH					
Wild type[#]	903	19.8×10^{-3}	1	652	3.3×10^{7}
Q118A	240	104×10^{-3}	5.3	173	1.7×10^{6}
Q118D	65	175×10^{-3}	8.9	47	2.7×10^{5}

The values for the wild-type OcDH were taken from Mueller *et al.*[16] Values for K_m and k_{cat} of the Gln118Ala and Gln118Asp mutants were determined by analyzing the data according to the Michaelis–Menten equation using the enzyme kinetic module 2.0 of Sigma Plot 9.0 (Systat Software).

[#] The values for the wild-type ODH were taken from Mueller *et al.*[16]

Table 5. Activity of different α-keto acid substrates

	V_{max} (μmol min^{-1} mg^{-1})	K_m (mmol L^{-1})	k_{cat} (s^{-1})	k_{cat}/K_m (L*$mmol^{-1}$ s^{-1})
Pyruvate	1074	0.77	775	1000
Ketobutyrate	728	5.9	526	90
Ketovalerate	377	49.8	272	5

Data for OcDH and pyruvate were taken from Mueller *et al.*[16] Values for K_m and k_{cat} of the different α-keto acids ketobutyrate and ketovalerate were determined by analyzing the data according to the Michaelis–Menten equation using Sigma Plot 9.0 (Systat Software) and the enzyme kinetic module 2.0.

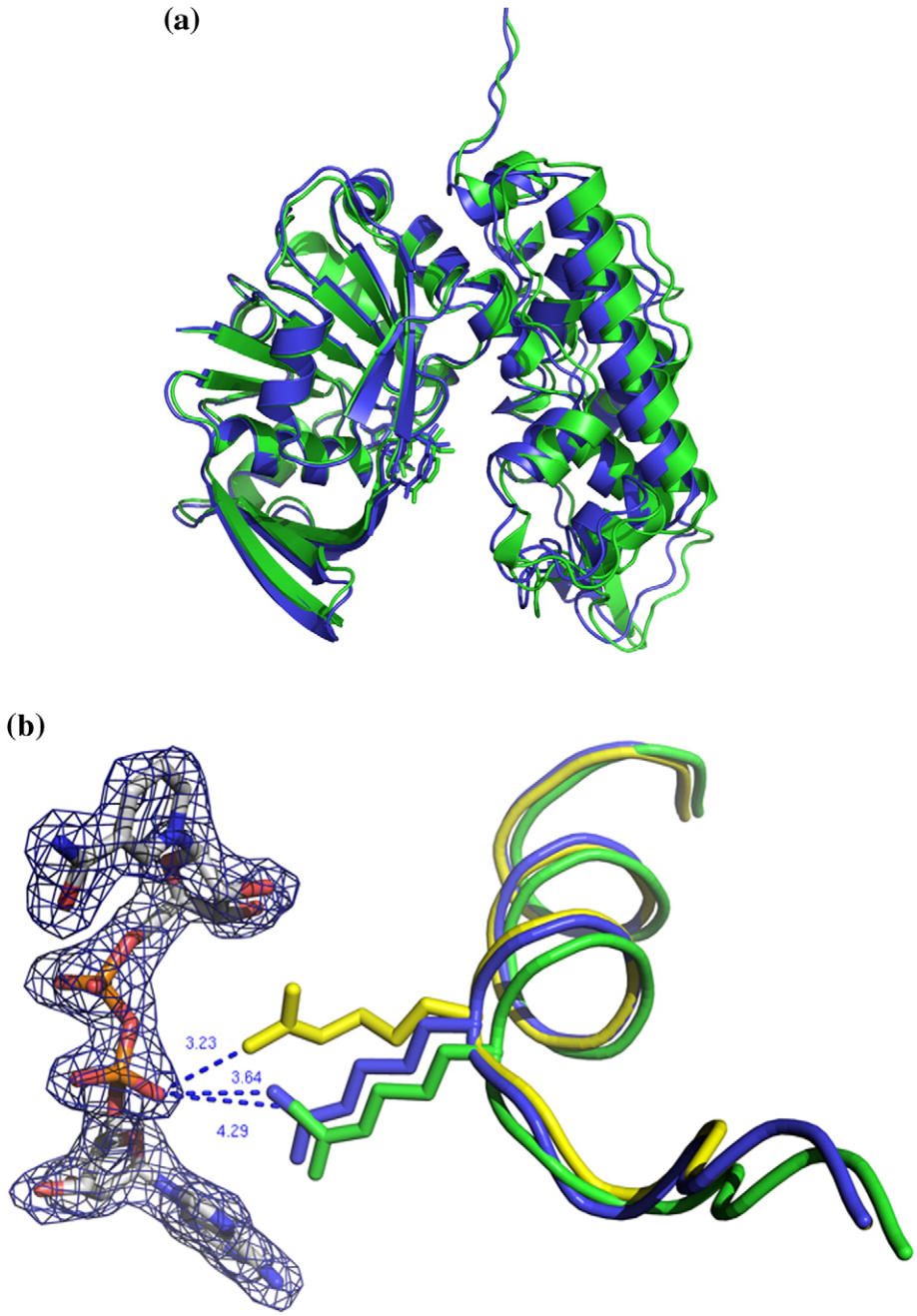

Fig. 4. The role of Arg324 in substrate-dependent domain closure. (a) Superpositions of the OcDH–NADH (green) and OcDH–NADH/L-arginine (blue) complexes highlight the inward rotation of domain II. The rmsd is 0.75° over 404 C^{α} atoms. (b) Superpositions of the OcDH–NADH (green), OcDH–NADH/L-arginine (blue) and OcDH–NADH/pyruvate (yellow) complexes. The interactions between NADH and Arg324 are highlighted, and the corresponding distances are shown. The final $2F_o - F_c$ electron density map for NADH of the binary OcDH–NADH structure contoured at 1σ is shown as a blue mesh.

hydride transfer can proceed. Thus, we propose that, instead of a random binding process, an ordered sequence of substrate binding in the line of NADH, L-arginine and pyruvate will occur. This sequential order of substrate binding might be the key to why pyruvate is not reduced to L-lactate *in vivo* and why opine formation has been preserved as a terminal step of anaerobiosis in some invertebrates during evolution.

Substrate specificity and stereoselectivity of OcDH

The results presented above provide new insights into the mechanism of OcDH and suggest a sequential binding order for all substrates. Furthermore, the syn conformation of NADH (Figs. 2 and 3) leads to a quantitative formation of the D-stereoisomer during the reductive condensation of L-arginine and pyruvate. However, important questions remain—how does OcDH ensure this amazingly high specificity for the L-arginine side chain and how is the L-isomer selected?

Surface potential calculation reveals a rather general distribution of charges in OcDH (Fig. 5a and b), but a highly negatively charged pocket, which harbors His212, is present inside the cleft between the two domains. This conspicuous structure might serve to absorb the positively charged guanidinium group of L-arginine. As other substrates, such as canavanine (25%), cysteine (1.2%), L-alanine (<1%), ornithine (<1%) and norvaline (<1%), display reduced or negligible activity (Table 6), the presence of this electrostatic sink capturing the highly positively charged guanidinium side chain of L-arginine ensures substrate selectivity. Furthermore, the length of the side chain of the amino acid substrate imposes restraints on the binding mode of the α-carboxy group of L-arginine. To ensure proper stereoselectivity within the reaction cycle of OcDH, we fixed the α-amino and α-carboxy groups via electrostatic interactions such that the positively charged α-amino group binds to the negatively charged pocket and the negatively charged α-carboxy group points away from the pocket toward the solvent (Figs. 2 and 5c), thereby preventing the binding of D-arginine. The specific interactions of OcDH with L-arginine provide the first level of substrate selection and stereoselection, but it is conceivable that the negatively charged cavity serves as an electrostatic sink acting as a molecular measuring device, a "charge ruler" that will guarantee that only L-arginine with the proper stereoconfiguration is recognized and tightly bound to OcDH for the subsequent reaction with pyruvate.

Table 6. Substrate specificity of recombinant wild-type OcDH

Substrate	Activity (U/mL)	Specific activity (U/mg)	Percentage
Arginine	12,678	634	100
Canavanine	3092	154.6	24.74
Cysteine	148	7.4	1.18
L-Alanine	35.1	1.8	0.29
Ornithine	32.3	1.6	0.26
Norvaline	3.0	0.95	0.15

Data for OcDH and arginine were taken from Mueller *et al.*[16] Activity and specific activity of the different substrates were determined as described in Materials and Methods.

The reductive condensation of pyruvate and L-arginine to octopine catalyzed by OcDH is mediated by a reaction mechanism requiring the involvement of both domains of this monomeric dehydrogenase. Biochemical data support the view that the reaction mechanism of all OpDHs proceeds via carbinolamine and imino acid intermediates.[41] However, the proposed catalytic triad composed of His212, Asp329 and Arg324 is in structural terms only a dyad, composed of the proton relay system His212–Asp329, while Arg324 represents the important sensor inducing domain closure via interaction with the pyrophosphate moiety of NADH. Thus, with the determination of principles of how OcDH ensures the reductive condensation of L-arginine with pyruvate and the identification of molecular rulers ensuring substrate selectivity and stereoselectivity,

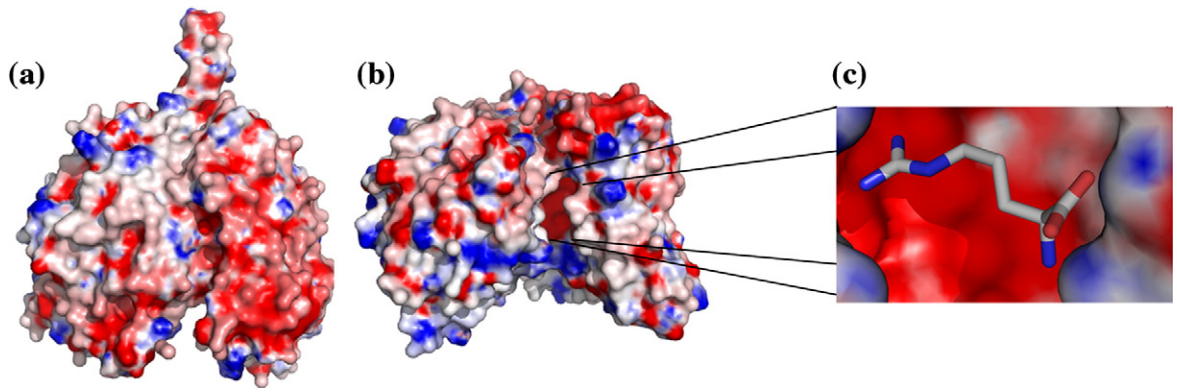

Fig. 5. Charge surface representation of the OcDH–NADH/L-arginine complex. (a) Front and (b) side representations after a 90° rotation perpendicular to the plane of the paper of the surface charges of OcDH. Here, a highly negatively charged pocket between the domains becomes visible. (c) Charge distribution within the L-arginine binding pocket (shown in stick representation). Red represents negative charges and blue represents positive charges contoured at 8 kT.

it will now be possible to employ OcDH as a framework for a rational design of different OpDHs for a general application of this fascinating enzyme family in biotechnology or enzyme-based chemical synthesis for drug development.

Materials and Methods

Expression and purification of recombinant OcDH-His$_5$ for crystallization

Cloning of the OcDH gene was performed as described previously.[16] For large-scale expression, *Escherichia coli* ER2566 cells harboring the plasmid pTYB1-OcDH-His$_5$ were grown at 37 °C in 8 L of LB medium containing 100 μg mL^{-1} of ampicillin until an optical density of 0.6 was reached. Expression of OcDH-His$_5$ was induced by adding 0.35 mM IPTG, and cultivation continued at 18 °C for 24 h. Cells were harvested and resuspended in lysis buffer (50 mM Na–phosphate buffer, pH 8.0, containing 300 mM NaCl and 10 mM imidazole) and disrupted by sonication (Bandelin, Berlin, Germany). After centrifugation for 60 min at 22,000*g* and 4 °C, the supernatant was subjected to a two-step ammonium sulfate precipitation. Solid ammonium sulfate was added to achieve 50% saturation. The solution was centrifuged for 1 h at 22,000*g* and 4 °C. The precipitate was discarded and ammonium sulfate was increased to a saturation of 80%. After centrifugation (1 h, 22,000*g*, 4 °C), the pellet was resuspended in lysis buffer and dialyzed against the same buffer for 12 h. The protein solution was applied to a Ni^{2+}–nitrilotriacetic acid column (Qiagen, Hilden, Germany). Unbound proteins were washed off the column with a Na–phosphate buffer (pH 8.0, 300 mM NaCl and 10 mM imidazole), followed by a second washing step with the same buffer but including 20 mM imidazole. Bound OcDH-His$_5$ was eluted using a linear gradient ranging from 40 to 250 mM imidazole. Fractions with the highest OcDH activity were pooled and concentrated using an Amicon cell with YM-10 filter membranes (10,000 MWCO; Millipore, Eschborn, Germany). The resulting solution was then chromatographed on a Sephadex G-100 column (bed volume = 145 cm × 7.5 cm), equilibrated with 50 mM Na,K–phosphate buffer, pH 7.5, containing 2 mM ethylenediaminetetraacetic acid, 10% (v/v) glycerol and 0.1% (v/v) mercaptoethanol. Peak fractions were pooled and concentrated as described above.

Expression and purification of selenomethionine-substituted OcDH

For selenomethionine substitution, *E. coli* B384(DE3) cells were grown in M9 minimal medium supplemented with 50 μg mL^{-1} of L-selenomethionine (Calbiochem, Darmstadt, Germany). Expression and purification were identical with those for native OcDH.

Site-directed mutagenesis

Site-directed mutagenesis was performed as already described[16] using the plasmid pTYBI-OcDH-His$_5$ as a template. Mutant plasmids were sequenced by Qiagen to ensure the correct DNA sequence of the constructs. Expression and purification of Q118 mutants were performed as for OcDH-His$_5$.

Enzyme assay

OcDH activity was measured spectrophotometrically at 25 °C following the decrease in absorbency at 339 nm. Standard assays were carried out using 3 mM pyruvate and 0.16 mM NADH in 50 mM triethanolamine buffer, pH 7.0. The reaction was started by the addition of 5.5 mM L-arginine. Activities were calculated using a specific absorbance coefficient, $\varepsilon = 6.31$ mM^{-1} cm^{-1}, for NADH. One unit is defined as the amount of enzyme catalyzing the oxidation of 1 μmol NADH per minute.

Determination of kinetic parameters

For the estimation of kinetic constants, the initial velocities at varied substrate concentrations of pyruvate, L-arginine and NADH were recorded spectrophotometrically at 339 nm. Kinetic parameters were obtained using nonlinear least-squares analysis of the data fitted to the Michaelis–Menten rate equation ($v = V_{max} \cdot [S]/K_m + [S]$) or the Michaelis–Menten equation corrected for uncompetitive substrate inhibition (where v is the velocity; V_{max}, the maximum velocity; S, the substrate concentration; K_m, the Michaelis constant; and K_i, the inhibition constant), using the enzyme kinetic module 2.0 of Sigma Plot 9.0 (Systat Software).

Crystallization of OcDH-His$_5$

Crystallization trials were carried out using the hanging-drop vapor diffusion method at 12 °C. Homogenous OcDH-His$_5$ was dialyzed against 10 mM Hepes, pH 7.0, containing 1 mM ethylenediaminetetraacetic acid and 1 mM DTT, and concentrated to 20 mg mL^{-1} prior to crystallization. For crystallization of OcDH with co-substrate, 0.8 mM NADH was added to the protein solution. Crystals were grown by mixing protein solution with a reservoir solution containing 100 mM Mes (4-morpholineethanesulfonic acid), pH 7.0, and Na–citrate ranging from 1.0 to 1.2 M in a 1:1 ratio. Crystals normally grew in 3–5 days. Suitable crystals were cryo-protected using 100 mM Mes, pH 7.0, 30% (v/v) ethylene glycol and 1.15 M Na–citrate and then frozen in liquid nitrogen. L-Arginine-bound crystals were obtained by soaking NADH-bound OcDH crystals in 100 mM Mes, pH 7.0, 1.15 M Na–citrate and 0.8 mM NADH containing 10 mM L-arginine for at least 24 h and then frozen as described before. Pyruvate-bound crystals were obtained also by soaking the crystals in 100 mM Mes, pH 7.0, 1.15 M Na–citrate, 0.8 mM NADH and 10 mM pyruvate for at least 8 h.

Data collection and structure determination

Data sets were collected at the BW7A (OcDH–NADH/pyruvate) and X12 (OcDH–NADH, OcDH–NADH/L-arginine) beamlines (EMBL, DESY Synchrotron, Hamburg, Germany). Detailed information on data collection statistics are shown in Table 1. A single SAD data set of OcDH–NADH protein crystals containing selenomethionine was collected at beamline X12 (EMBL, DESY) at a resolution of 2.8 Å. For all data sets, the optimal data collection strategy was calculated using the program BEST.[42] All data sets were processed with DENZO[17] or the XDS program packages. The selenomethionine positions and, afterward, initial phases were determined and automated model building was performed using the program Auto-Rickshaw.[19] Eleven of the 12 possible selenomethionine sites were initially found.

The model was then further refined using REFMAC5[18] and Coot,[21] resulting in a complete model of the OcDH–NADH complex. This model was applied as a template to phase the high-resolution data set of OcDH at 2.1 Å using the molecular replacement program Phaser.[43] The quality of the electron density allowed automatic water picking using Arp/Warp,[22] which was manually checked on correct assignment. Two other data sets were collected, OcDH–NADH/L-arginine at 3.1 Å and OcDH–NADH/pyruvate at 2.6 Å. These data sets were phased using the molecular replacement program Phaser[43] and further refined using REFMAC5[18] and Coot.[21] Refinement statistics are listed in Table 1. In the OcDH–NADH/pyruvate structure, however, the density of one loop (amino acids 281–290) was poor and no side chain could be modeled. This loop is involved in crystal contacts and was excluded from the final model.

Figure preparation

Structured figures were prepared using PyMol‡.

Accession codes

Coordinates have been deposited in the Protein Data Bank under accession codes 3C7A (OcDH–NADH), 3C7C (OcDH–NADH/L-arginine) and 3C7D (OcDH–NADH/pyruvate).

Acknowledgements

This work was supported by Deutsche Forschungsgemeinschaft (grant GR456/20-4 to M.K.G.). We thank Drs. Matthew Grooves and Paul Tucker for their excellent support at the beamlines of the EMBL Hamburg Outstation as well as Barbara Bartosinska and Silke Jakob for their expert technical assistance. We also thank Dr. Ulrich Schulte for stimulating discussions and critical reading of the manuscript.

References

1. Thomas, G. E. & Gruffyd, L. I. D. (1971). The type of escape reactions elicited in the scallop *Pecten maximus* by selected sea star species. *Mar. Biol.* **10**, 87–93.
2. Grieshaber, M. K., Hardewig, I., Kreutzer, U. & Portner, H. O. (1994). Physiological and metabolic responses to hypoxia in invertebrates. *Rev. Physiol., Biochem. Pharmacol.* **125**, 43–147.
3. Thoai, N. V. & Robin, Y. (1959). On the biogenesis of octopine in different tissues of *Pecten maximus*. *Bull. Soc. Chim. Biol. (Paris)*, **41**, 735–742.
4. Thompson, J. & Donkersloot, J. A. (1992). *N*-(Carboxyalkyl)amino acids: occurrence, synthesis, and functions. *Annu. Rev. Biochem.* **61**, 517–557.
5. Thompson, J. & Miller, S. P. (1988). N^6-(1-carboxyethyl)lysine formation by *Streptococcus lactis*. Purification, synthesis, and stereochemical structure. *J. Biol. Chem.* **263**, 2064–2069.
6. Miller, S. P. & Thompson, J. (1987). Biosynthesis and stereochemical configuration of N^5-(1-carboxyethyl) ornithine. An unusual amino acid produced by *Streptococcus lactis*. *J. Biol. Chem.* **262**, 16109–16115.
7. Nishida, H., Nishiyama, M., Kobashi, N., Kosuge, T., Hoshino, T. & Yamane, H. (1999). A prokaryotic gene cluster involved in synthesis of lysine through the amino adipate pathway: a key to the evolution of amino acid biosynthesis. *Genome Res.* **9**, 1175–1183.
8. Chilton, M. D., Drummond, M. H., Merio, D. J., Sciaky, D., Montoya, A. L., Gordon, M. P. & Nester, E. W. (1977). Stable incorporation of plasmid DNA into higher plant cells: the molecular basis of crown gall tumorigenesis. *Cell*, **11**, 263–271.
9. Veluthambi, K., Krishnan, M., Gould, J. H., Smith, R. H. & Gelvin, S. B. (1989). Opines stimulate induction of the vir genes of the *Agrobacterium tumefaciens* Ti plasmid. *J. Bacteriol.* **171**, 3696–3703.
10. Endo, N., Kan-no, N. & Nagahisa, E. (2007). Purification, characterization, and cDNA cloning of opine dehydrogenases from the polychaete rockworm *Marphysa sanguinea*. *Comp. Biochem. Physiol., Part B: Biochem. Mol. Biol.* **147**, 293–307.
11. Kato, Y., Yamada, H. & Asano, Y. (1996). Stereoselective synthesis of opine-type secondary amine carboxylic acids by a new enzyme opine dehydrogenase. *J. Mol. Catal. B: Enzym.* **1**, 151–160.
12. van Thoai, N., Huc, C., Pho, D. B. & Olomucki, A. (1969). Octopine dehydrogenase. Purification and catalytic properties. *Biochim. Biophys. Acta*, **191**, 46–57.
13. Gade, G. & Grieshaber, M. (1986). Pyruvate reductases catalyze the formation of lactate and opines in anaerobic invertebrates. *Comp. Biochem. Physiol., Part B: Biochem. Mol. Biol.* **83**, 255–272.
14. Carvajal, N. & Kessi, E. (1988). Kinetic mechanism of octopine dehydrogenase from the muscle of the sea mollusc, *Concholepas concholepas*. *Biochim. Biophys. Acta*, **953**, 14–19.
15. Thompson, J. & Miller, S. P. (1991). N^5-(1-carboxyethyl)ornithine and related *N*-carboxyalkyl-amino acids: structure, biosynthesis, and function. *Adv. Enzymol. Relat. Areas Mol. Biol.* **64**, 317–399.
16. Mueller, A., Janssen, F. & Grieshaber, M. K. (2007). Putative reaction mechanism of heterologously expressed octopine dehydrogenase from the great scallop, *Pecten maximus*. *FEBS J.* **274**, 6329–6339.
17. Otwinowski, Z. & Minor, W. (1997). Processing of X-ray diffraction data collected in oscillation mode. In (Carter, C. W. & Sweet, R. M., eds), *Methods in Enzymology*, Vol. 276. Academic Press, London.
18. Murshudov, G., Vagin, A. A. & Dodson, E. J. (1997). Refinement of macromolecular structures by the maximum-likelihood method. *Acta Crystallogr., Sect. D: Biol. Crystallogr.* **53**, 240–255.
19. Panjikar, S., Parthasarathy, V., Lamzin, V. S., Weiss, M. S. & Tucker, P. A. (2005). Auto-Rickshaw: an automated crystal structure determination platform as an efficient tool for the validation of an X-ray diffraction experiment. *Acta Crystallogr., Sect. D: Biol. Crystallogr.* **61**, 449–457.
20. Laskowski, R. A., MacArthur, M. W., Moss, D. S. & Thornton, J. M. (1993). PROCHECK: a program to check the stereochemical quality of protein structures. *J. Appl. Crystallogr.* **26**, 283–291.
21. Emsley, P. & Cowtan, K. (2004). Coot: model-building tools for molecular graphics. *Acta Crystallogr., Sect. D: Biol. Crystallogr.* **60**, 2126–2132.
22. Lamzin, V. S. & Wilson, K. S. (1993). Automated refinement of protein models. *Acta Crystallogr., Sect. D: Biol. Crystallogr.* **49**, 129–147.

‡ http://pymol.sourceforge.net/

23. Rossmann, M. G., Moras, D. & Olsen, K. W. (1974). Chemical and biological evolution of nucleotide-binding protein. *Nature*, **250**, 194–199.
24. Bashton, M. & Chothia, C. (2002). The geometry of domain combination in proteins. *J. Mol. Biol.* **315**, 927–939.
25. Schulz, G. E. (1992). Binding of nucleotide by proteins. *Curr. Opin. Struct. Biol.* **2**, 61–67.
26. Stockwell, G. R. & Thornton, J. M. (2006). Conformational diversity of ligands bound to proteins. *J. Mol. Biol.* **356**, 928–944.
27. Biellmann, J. F., Branlant, G. & Olomucki, A. (1973). Stereochemistry of the hydrogen transfer to the coenzyme by octopine dehydrogenase. *FEBS Lett.* **32**, 254–256.
28. Storey, K. B. & Dando, P. R. (1982). Substrate specificities of octopine dehydrogenases from marine invertebrates. *Comp. Biochem. Physiol., Part B: Biochem. Mol. Biol.*, 521–528.
29. Schrimsher, J. L. & Taylor, K. B. (1984). Octopine dehydrogenase from *Pecten maximus*: steady-state mechanism. *Biochemistry*, **23**, 1348–1353.
30. Clarke, A. R., Wilks, H. M., Barstow, D. A., Atkinson, T., Chia, W. N. & Holbrook, J. J. (1988). An investigation of the contribution made by the carboxylate group of an active site histidine–aspartate couple to binding and catalysis in lactate dehydrogenase. *Biochemistry*, **27**, 1617–1622.
31. Goward, C. R. & Nicholls, D. J. (1994). Malate dehydrogenase: a model for structure, evolution, and catalysis. *Protein Sci.* **3**, 1883–1888.
32. Britton, K. L., Asano, Y. & Rice, D. W. (1998). Crystal structure and active site location of *N*-(1-D-carboxylethyl)-L-norvaline dehydrogenase. *Nat. Struct. Biol.* **5**, 593–601.
33. Asano, Y., Yamaguchi, K. & Kondo, K. (1989). A new NAD^+-dependent opine dehydrogenase from *Arthrobacter* sp. strain 1C. *J. Bacteriol.* **171**, 4466–4471.
34. Dairi, T. & Asano, Y. (1995). Cloning, nucleotide sequencing, and expression of an opine dehydrogenase gene from *Arthrobacter* sp. strain 1C. *Appl. Environ. Microbiol.* **61**, 3169–3171.
35. Holm, L. & Park, J. (2000). DaliLite workbench for protein structure comparison. *Bioinformatics*, **16**, 566–567.
36. Andi, B., Xu, H., Cook, P. F. & West, A. H. (2007). Crystal structures of ligand-bound saccharopine dehydrogenase from *Saccharomyces cerevisiae*. *Biochemistry*, **46**, 12512–12521.
37. Burk, D. L., Hwang, J., Kwok, E., Marrone, L., Goodfellow, V., Dmitrienko, G. I. & Berghuis, A. M. (2007). Structural studies of the final enzyme in the alpha-aminoadipate pathway-saccharopine dehydrogenase from *Saccharomyces cerevisiae*. *J. Mol. Biol.* **373**, 745–754.
38. Hayward, S. & Lee, R. A. (2002). Improvements in the analysis of domain motions in proteins from conformational change: DynDom version 1.50. *J. Mol. Graphics Modell.* **21**, 181–183.
39. Hayward, S. & Kitao, A. (2006). Molecular dynamics simulations of NAD^+-induced domain closure in horse liver alcohol dehydrogenase. *Biophys. J.* **91**, 1823–1831.
40. Gerstein, M., Lesk, A. M. & Chothia, C. (1994). Structural mechanisms for domain movements in proteins. *Biochemistry*, **33**, 6739–6749.
41. Stillman, T. J., Baker, P. J., Britton, K. L. & Rice, D. W. (1993). Conformational flexibility in glutamate dehydrogenase. Role of water in substrate recognition and catalysis. *J. Mol. Biol.* **234**, 1131–1139.
42. Popov, A. N. & Bourenkov, G. P. (2003). Choice of data-collection parameters based on statistic modelling. *Acta Crystallogr., Sect. D: Biol. Crystallogr.* **59**, 1145–1153.
43. McCoy, A. J., Grosse-Kunstleve, R. W., Adams, P. D., Winn, M. D., Storoni, L. C. & Read, R. J. (2007). Phaser crystallographic software. *J. Appl. Crystallogr.* **40**, 658–674.